Journal of Computational Chemistry

WILEY

Journal of COMPUTATIONAL CHEMISTRY

RESEARCH ARTICLE OPEN ACCESS

Density Functional Theory (DFT) and Time-Dependent DFT (TDDFT) Studies of Porphyrin Adsorption on Graphene: Insights on the Effect of Substituents and Central Metal on Adsorption Energies

Rayene Gara[1] | Ángel Morales-García[2] | Youssef Arfaoui[1] | Francesc Illas[2]

[1]Laboratory of Characterizations, Applications & Modeling of Materials (LR18ES08), Department of Chemistry, Faculty of Sciences of Tunis, University of Tunis El Manar, Tunis, Tunisia | [2]Departament de Química Física and Institut de Química Teorica i Computacional (IQTCUB), Universitat de Barcelona, Barcelona, Spain

Correspondence: Ángel Morales-García (angel.morales@ub.edu)

Received: 19 July 2024 | **Revised:** 24 October 2024 | **Accepted:** 27 October 2024

Funding: We thank the financial support from MCIN/AEI/10.13039/501100011033 through projects PID2020-115293RJ-I00, PID2021-126076NB-I00, TED2021-129506B-C22, and the María de Maeztu CEX2021-001202-M project, and, in part, from the Generalitat de Catalunya through the 2021-SGR-00079 grant. The reported research is also involved in the European Cooperation in Science and Technology (COST) Actions: CA18234.

Keywords: adsoprtion energy | optoelectronic properties | TDDFT porphyrin graphene

ABSTRACT

Combining metalloporphyrins (MPr) and graphene constitutes key composites in the development of photovoltaic devices. Here, we focus on the analysis of the properties of metalloporphyrins/graphene systems by means of the density functional theory (DFT) and its time-dependent (TDDFT) version, focusing on the ground and singlet excited states. Our benchmark analysis concludes that ωB97XD density functional combined with 6-31G(d)/Def2-TZVP basis set is a better-suited method for simulating accurate MPr adsorption on graphene. It is shown that a reduced atomic model where the external organic shell of the structure is removed provides the same resulting optoelectronic properties of the original model, constituting an important speed-up of the calculations when studying porphyrins-derived molecules. We observe that ZnPr provides the highest light harvesting efficiency (LHE) value. In addition, we find out that the adsorption energy increases monotonically with the size of the graphene flake and the highest stability involves the use of graphene comprising above 500 atoms. Besides, CdPr and HgPr keep their properties as photosensitizers when they are bonded to graphene and show promising values in terms of LHE emerging as suitable solar energy harvesters.

1 | Introduction

Graphene has attracted significant attention in recent years due to its exceptional electronic, optical, and mechanical properties [1–4]. Expanding the potential applications of graphene, particularly in the realm of optoelectronic devices and energy conversion systems, has prompted extensive research into the interactions between graphene surfaces and organic molecules. More precisely, the noncovalent adsorption of conjugated organic molecules on graphene, facilitated by π–π interactions, is a promising soft approach to modifying the electronic properties of graphene without compromising its structure [5]. Currently, research is focused on designing new systems to control both the interaction and the electronic properties of graphene [6–9]. Porphyrins (Pr) and phthalocyanines (Pc) have emerged as suitable candidates for surface adsorption studies due to their unique electronic and structural properties with implications in catalysis, sensing, and photovoltaics [10–13].

In this context, investigating the properties of Pr and Pc adsorbed on graphene surfaces has become the spotlight in the exploration and development of organic photovoltaic solar cells (OPVs) applications [14–16]. In this sense, it is worth noting that the adsorption of organic pigments on graphene can lead to modifications in the electronic and optical properties of the system [17]. These organic pigments have the ability to introduce electrons or holes into graphene, thereby altering its conductivity. Additionally, the adsorption of organic pigments can influence light absorption and emission, which is crucial for optoelectronic applications and photovoltaic devices. The present study critically examines recent advancements and challenges in understanding the adsorption mechanisms and electronic modifications resulting from interactions between these prominent organic molecules and graphene layers. Through a comprehensive analysis of experimental and theoretical studies, we aim to provide insights into the interplay between molecular structures and electronic properties, contributing to the design and optimization of graphene-based devices for OPVs.

Considering the complexity of the features of the organic pigment-graphene combined system, our aim is also to evaluate the light-harvesting ability of systems arising from combining metalloporphyrins and metallophthalocyanines with graphene. To this end, a series of models are designed and their geometric structures are optimized by means of a suited density functional theory (DFT) method. Finally, the optical absorption properties are investigated through the time-dependent density functional theory (TDDFT) method in light of previous experimental reports.

2 | Computational Methods and Models

Zinc containing phthalocyanine and porphyrin heterocyclic compounds are selected to inspect their properties and how they vary when adsorbed on graphene. Phthalocyanines have a square planar structure and are highly conjugated and employed as optoelectronic-derived materials, while porphyrins are characterized by a tetrapyrrolic macrocycle playing a crucial role in oxygen transport and catalysis. The atomic models of the full Zn-phthalocyanine (ZnPccor4) and Zn-porphyrin (ZnPrcor4) are depicted in Figure 1. The choice of crown ethers moieties is justified by the fact that they do not affect the optoelectronic properties of ZnPc and ZnPr while playing a dual ecological role: absorbing light and capturing both heavy metals and alkali metals, as reported in previous works theoretically [18] and experimentally [19–21]. To facilitate the study of the excited states of these compounds adsorbed, simplified models have been designed where the external crown ethers are systematically removed, as described below. The resulting simplified models with the four-crown ether removed are also depicted in Figure 1.

All quantum chemical calculations were performed in the framework of the density functional theory (DFT) as implemented in GAUSSIAN16 software [22]. In addition, the Gauss View 6 molecular program was employed for visualizing and analyzing the Gaussian outputs [23]. To select a suited theoretical approach for studying the adsorption of complexes on graphene, a benchmark analysis was first carried out using a set of density functionals including hybrid B3LYP, [24, 25] CAM-B3LYP [26], meta-hybrid M06 and M06-2X [27], and long-range separated ωB97XD [28, 29], and different basis sets such as 3-21G [30], 6-31G(d) [31], 6-311G(d,p) [32], cc-PVDZ [33], cc-PVTZ [34], LANL2DZ [35], LANL2TZ [36], and def2TZVP [37]. In addition, the solvent effect was also included by considering the polarizable continuum model (PCM) [38–40]. The study of the solvent effect revealed that chloroform admits the highest absorbance value and the lowest energy gap (Table 1). Several structural optimization options have been used to obtain a model of the simplified (phthalocyanine and porphyrin) pigment. The "opt = loose" keyword proved to be helpful in speeding up the optimization process. It should be noted that "opt = loose" defines the optimization convergence criteria with a maximum step size of 0.01 u [41].

For the optimized structures, the electronic properties are investigated focusing first on the HOMO–LUMO gap [42, 43] as a measure of the electron injection during the operation of the photovoltaic organic solar cell. In fact, there are two possible pathways for electron injection, and the levels of frontier molecular orbitals are important for a better understanding of pigment performance. To simulate the UV absorption spectra, the first 30 electronic excitation energies with the lowest energy ΔE_{0-n} (n denotes the excited state in the 1–30 range, while 0 stands for the ground one) were computed using the time-dependent perturbation approach to TDDFT [44–46]. To illustrate the photoelectric properties of the studied compounds, we have focused on defining the corresponding electronic absorption parameters, including light-harvesting efficiency (LHE), oscillator strength (f), and maximum absorbance wavelength (λ_{max}) values. It is important to mention that LHE refers to the efficiency with which a light-harvesting system, such as a photovoltaic device, captures and utilizes light energy. In photovoltaic systems, it is a measure of how effectively solar cells capture sunlight and convert it into electrical energy. It can be calculated based on the absorption spectrum of the material and the incident light spectrum. The former is expressed as:

$$\mathrm{LHE} = 1 - 10^{-f} \tag{1}$$

For an additional statistical analysis, the mean absolute deviation (MAD) [47] is selected by comparing it to available experimental results. This statistical parameter determines the average magnitude of the deviations between the predicted and observed values, thereby providing insights into the precision and effectiveness of the methods being used. MAD is defined as,

$$\mathrm{MAD} = \sum_{i}^{N_{\mathrm{porphyrin}}} \frac{\left|E_v(i) - E_v(\mathrm{exp})\right|}{N} \tag{2}$$

where $E_v(i)$ represents the value of the theoretical vertical excitation energy of a given system (i) and $E_v(\mathrm{exp})$ is the value of the experimentally measured vertical energy.

From a thermodynamic point of view, the adsorption energy quantifies the interaction between an adsorbate and a surface. This allows one to evaluate whether the adsorption is favorable (or exothermic) or not (or endothermic). The adsorption energies

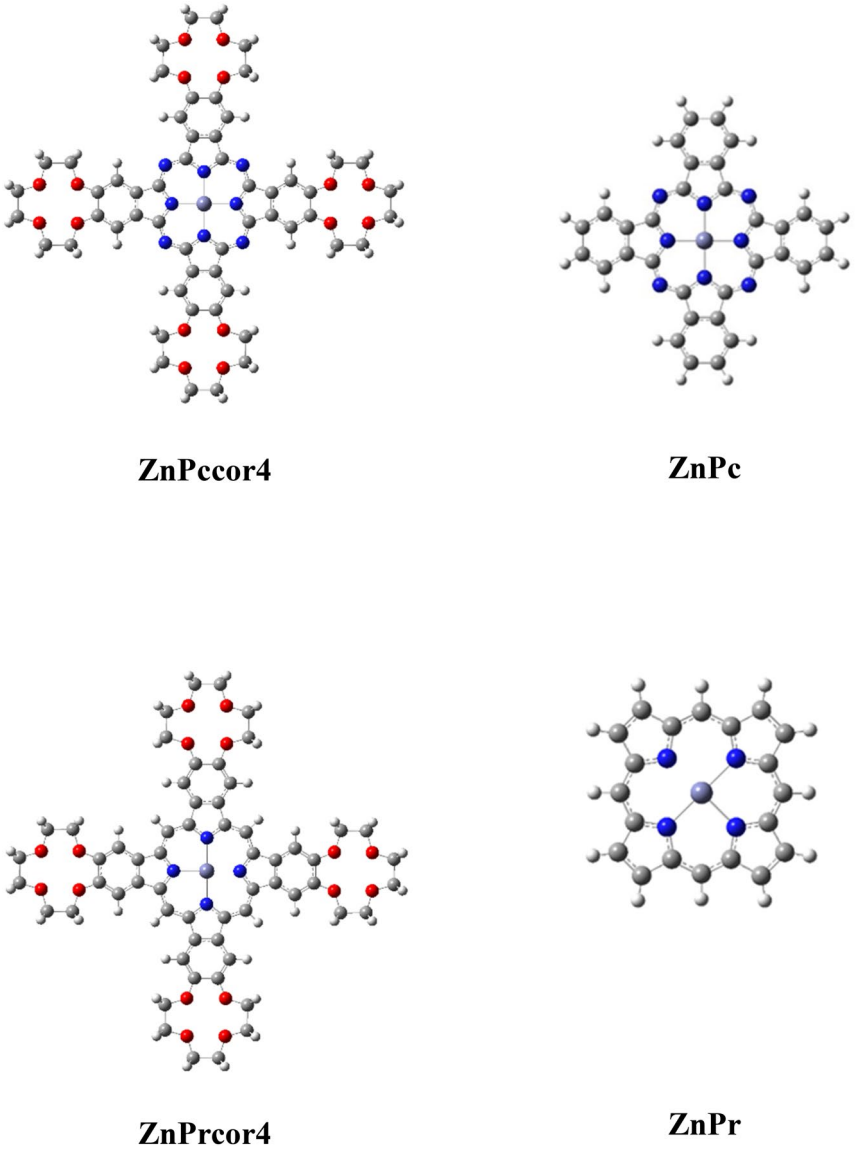

FIGURE 1 | Atomic representation of ZnPccor4 and ZnPrcor4 and their simplified models ZnPc and ZnPr, where the four crown ether have been removed, respectively. Light purple, blue, gray, white, and red spheres represent Zn, N, C, H, and O atoms, respectively.

(E_{ads}) and the contribution of the basis set superposition error (E_{ads}^{BSSE}) using the standard counterpoise method, [48, 49] of the metalloporphyrin (MPr) on a graphene (G) surface are listed in Table 7. BSSE is required when the employed basis set for different interacting fragments overlap with each other, leading to an overestimation of the interaction energy. Thus, the inclusion of this energetic term provides a more accurate estimation of the interaction strength between interacting systems, without the artificial overestimation due to the basis set superposition. The adsorption energy is then defined as:

$$E_{ads} = E(\mathrm{MPr/G}) - [E(\mathrm{MPr}) + E(\mathrm{G})] \quad (3)$$

$$E_{ads}^{BSSE} = E_{ads} + E^{BSSE} \quad (4)$$

where E(MPr/G) represents the total energy of the graphene with the supported MPr molecule, E(MPr) is the total energy of the isolated porphyrin, and E(G) is the total energy of the graphene layer. Finally, E^{BSSE} stands for the energetic contribution of the basis set superposition error. The graphene substrate, with a zigzag edge configuration, is represented by a sufficiently large flake, with the edge atoms saturated by H atoms. It should be mentioned that the dimensions of the graphene layer are approximately on the order of 13.6 Å. The influence of the size of the graphene flake on the adsorption energy is also considered for further study.

Before closing this section, we want to note that B3LYP density function works well describing the structural properties of ZnPc and ZnPr as discussed later. However, more sophisticated density functionals such as ωB97XD are required to describe accurately the electronic properties of such systems. Indeed, since the latter functional accounts for dispersion, it allows us also to explore the properties of the investigated systems supported on graphene, as discussed below (Figure 2).

TABLE 1 | Frontier molecular orbital energies HOMO and LUMO (i.e., $\varepsilon_H, \varepsilon_L$) in eV, fundamental gap energy (E_g) in eV, oscillator strength (f), and light-harvesting efficiency (LHE) for ZnPr calculated for in various solvents at the DFT/B3LYP/6-31G(d,p) level.

Solvent	ε_H	ε_L	E_g	f	LHE
H_2O	−4.84	−2.73	2.11	0.50	0.68
Chloroform	−4.83	−2.71	2.13	0.56	0.72
DMSO	−4.67	−2.53	2.14	0.55	0.71
Dichloromethane	−4.75	−1.53	2.13	0.54	0.71
Cyclohexane	−4.47	−2.32	2.15	0.56	0.72
Acetone	−4.81	−2.68	2.13	0.51	0.69
CCl_4	−4.50	−2.35	2.15	0.52	0.70
Methanol	−4.82	−2.70	2.13	0.49	0.68

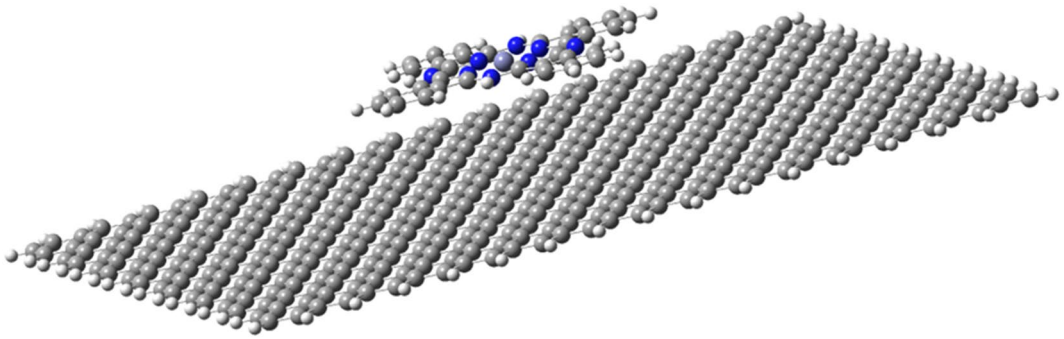

FIGURE 2 | Atomistic model of ZnPc/G System. Carbon atoms are shown in gray, hydrogen in white, oxygen in blue, and zinc in purple. Note that graphene is represented by a finite flake consisting of 512 C and 62 H atoms featuring a zigzag-edged lattice.

3 | Results and Discussion

3.1 | Effect of the Number of Crown Ethers

We start this section by analyzing the influence of using reduced atomic models for phthalocyanine and porphyrin [50]. In the simplified models, the external crown ethers of the initial ZnPc4cor and ZnPr4cor structure are removed one at a time, thus reducing the dimensionality of the atomic model. In this way, models with three crowns (labeled as ZnPc3cor and ZnPr3cor), two crowns (labeled as ZnPc2cor and ZnPr2cor), and one crown (labeled as ZnPc1cor and ZnPr1cor) are obtained. In the ZnPc and ZnPr models in Figure 1, the four-crown ethers have been removed.

Table 2 summarizes the main electronic structure properties, including frontier molecular orbital energies (i.e., ε_H, ε_L), fundamental energy gap (i.e., E_{gap}), oscillator strength (i.e., f), and LHE. ZnPr4cor exhibits a higher energy gap and oscillator strength than ZnPc4cor. Regardless of the composition, ε_H, ε_L, E_{gap}, f, and LHE parameters remain unaltered upon successively removing the crown ethers. This is an important result as indicates that this reduction of the system size has a negligible effect on the electronic properties of interest. This allows one to simplify the atomic structures to both minimize the computational cost and uncover key relationships between the structural modifications and their corresponding properties but, more importantly, it provides reliable models to investigate the electronic structure of these systems supported on graphene and, in this way, obtain information about the electronic structure modifications induced by the graphene support. This approach allowed for a clear assessment of the intrinsic electronic properties without introducing additional structural complexity. While the crown-ether groups do not alter these core properties, their potential impact on interactions with graphene was not explored in this work and remains a subject for future investigation. Further

TABLE 2 | Frontier molecular orbital energies HOMO and LUMO (i.e., $\varepsilon_H, \varepsilon_L$) in eV, fundamental gap energy (E_g) in eV, oscillator strength (f), and light-harvesting efficiency (LHE) calculated at the DFT/B3LYP/6-31G(d,p) level with CPCM (i.e., chloroform).

Compound	ε_H	ε_L	E_g	f	LHE
ZnPc4cor	−4.59	−2.41	2.18	1.22	0.94
ZnPc3cor	−4.58	−2.40	2.18	1.22	0.94
ZnPc2cor	−4.58	−2.39	2.19	1.23	0.94
ZnPc1cor	−4.59	−2.41	2.19	1.33	0.94
ZnPr4cor	−4.32	−1.79	2.53	3.50	0.99
ZnPr3cor	−4.32	−1.79	2.53	3.50	0.99
ZnPr2cor	−4.32	−1.78	2.54	3.40	0.99
ZnPr1cor	−4.32	−1.78	2.53	3.40	0.99

research will aim to examine the role of crown-ether groups in modulating the interactions between these compounds and graphene.

TABLE 3 | Structural parameters of ZnPc and ZnPr calculated at the DFT/B3LYP/6-31G(d,p) level with CPCM (i.e., chloroform).

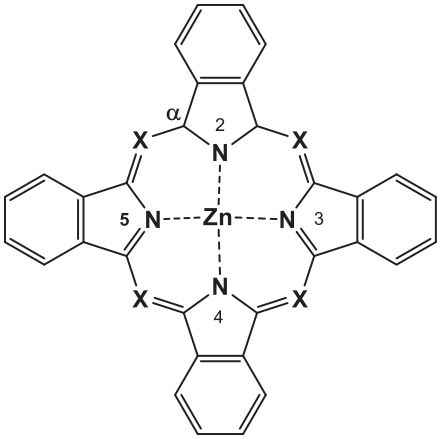

Structural parameter	ZnPc	ZnPr
d(Zn–N)[a]	2.001	2.067
	2.024 [52]	2.050 [53]
d(N–N)[b]	3.982	4.134
d(C–N_{ring})[c]	1.373	1.371
	1.368 [52]	1.372 [53]
d(C–X_{linker})[d]	1.333	1.376
α(N–Zn–N)[e]	90.0	90.0
α(C_α–N–C_α)[f]	108	107
	108.8 [52]	106.8 [53]

Note: Atomic model is included to facilitate the location of the structural parameter listed in the table. Average distances d in (Å) and α angles in degrees as well as values from the literature are included. Experimental data from Refs. [52, 53].
[a]Zn–N distance.
[b]N2–N4 and N3–N5 distances.
[c]C–N_{ring}.
[d]C–X_{linker}.
[e]N–Zn–N angle.
[f]C_α–N–C_α angle.

Additional results of ZnPc and ZnPr excited state and geometric properties were also analyzed. A strong correlation is observed between the calculated theoretical values for bond angles and lengths and the corresponding experimental measurements [51, 52] as shown in Table 3, thereby validating the adequacy of the selected computational approach. Table 4 summarizes the computed maximum absorption wavelengths (λ_{max}), vertical excitation energies (E_v) from the ground state to the first excited state, oscillator strengths (f), and transitions nature. Both compounds exhibit absorption within the visible range (432–633 nm), crucial for high efficiency (Figure 3). The primary focus is on determining LHE notably influenced by the intensity of light absorption. Vertical excitation energy, derived from λ_{max}, also plays a significant role. Higher LHE values are desirable for maximizing photocurrent response, with ZnPr exhibiting superior optoelectronic properties, boasting the highest LHE value of 0.99. Notably, transitioning from ZnPc to ZnPr results in a remarkable increase in oscillator strength. This result confirms the preferential choice of porphyrin.

3.2 | The Effect of Graphene as Support

Next, we investigate the effect of the graphene acting as support. Thus, we first analyze the interaction between either ZnPr or ZnPc with graphene acting as support. To obtain the equilibrium geometry of the combined system, we start optimizing the isolated graphene model. Subsequently, using this geometry as a starting point, we add the ZnPr and ZnPc monomers to the graphene center and then re-optimize the structure. Once the geometric optimization is completed, calculations of vibrational frequencies are performed to ensure that the optimized systems correspond to a minimum in the potential energy surface. For the ZnPr system, the B3LYP functional with the 6-31G(d,p) basis set did not provide energy gap values close to the experimental value of 0.1 eV [53] (Table 5), which is contrary to previous findings [18]. However, with this basis set, the ωB97XD functional already leads to an energy gap close to the experimental one [54, 55]. Therefore, the ωB97XD density functional is chosen to model these systems. A plausible explanation of the good performance of this functional in predicting the band gap of the ZnPr system is the inclusion of range-separation and Grimme's dispersion correction terms [56, 57]. To better justify

TABLE 4 | Calculated maximum absorption wavelengths (λ_{DFT}), dominant MO pairs involved in excitations, where H and L are abbreviations of HOMO and LOMO, respectively; vertical transition energies (E_v), oscillator strengths (f), and light-harvesting efficiencies (LHE) of ZnPc and ZnPr at the B3LYP/6-31G(d,p)/CPCM (chloroform) level.

Compound	λ_{DFT} (nm)	MOs	E_v (eV)	f	LHE
ZnPc	633	H–L + 1 (93%) H–L (93%)	1.95	1.22	0.93
	478	H-3–L (90%) H-3–L + 1 (90%)	2.61	1.12	
ZnPr	594	H–L (83%) H–L + 1 (83%)	2.10	0.64	0.99
	421	H-2–L + 1 (41%); H-- 1–L + 1 (49%) H-2–L (42%); H-1–L (48%) H-2–L (54%)	2.91 2.95	3.5	

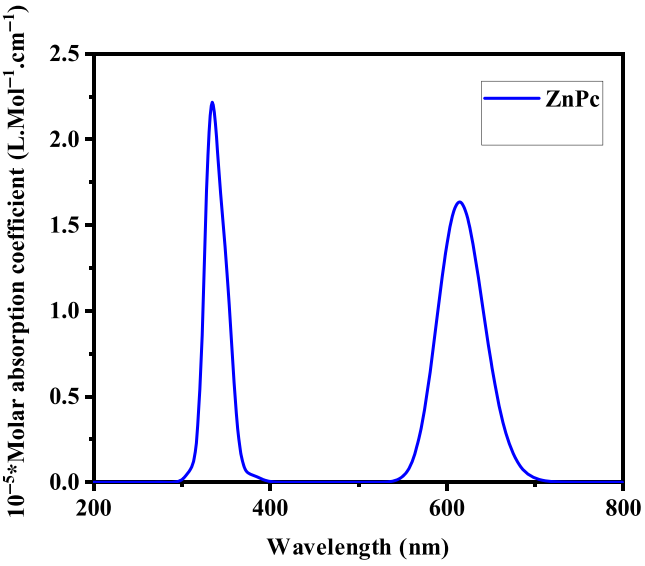

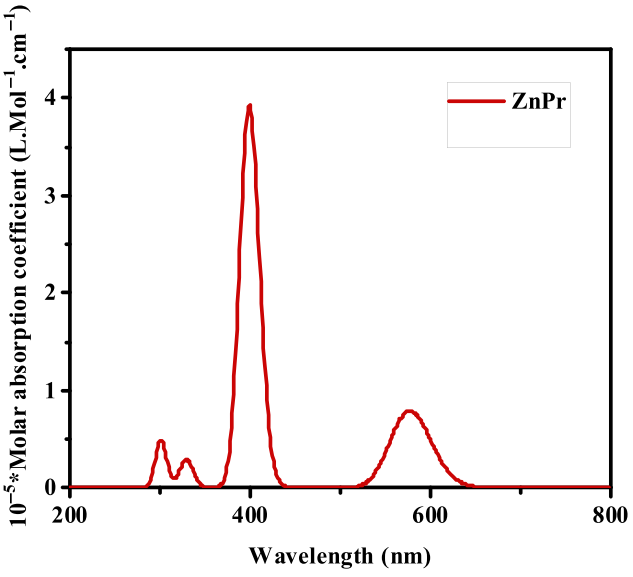

FIGURE 3 | Simulated UV–vis absorption spectra of ZnPc (blue) and ZnPr (red) as predicted from TDDFT at the B3LYP/6-31G(d,p)/CPCM (Chloroform) level of theory.

TABLE 5 | Calculated gap energy values of ZnPr using the 6-31G(d,p) basis and the indicated functional.

Functional	E_g (eV)
B3LYP	1.19
CAM-B3LYP	1.41
ωB97XD	0.20
M06	1.82
M06-2X	1.60

Note: Note that the experimental value is 0.1 eV [60].

our choice, we show the MAD analysis (Figure 4) for different density functionals by comparing the experimental and computational results of the vertical energies of the Q_x and Q_y bands, respectively [58–60]. The latter refers to transitions associated

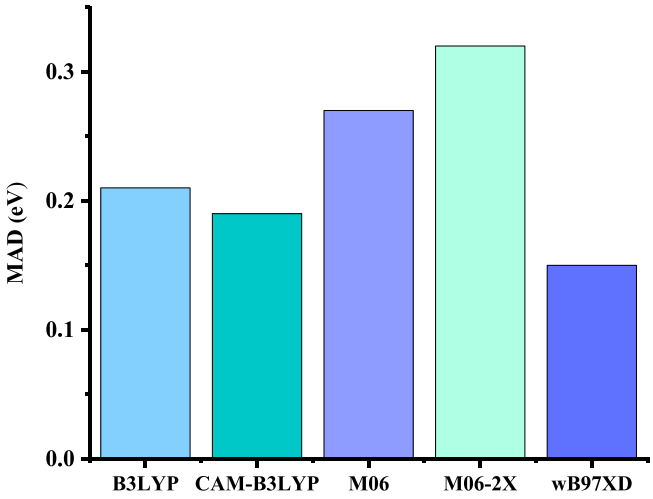

FIGURE 4 | Mean absolute deviation (MAD) comparison of the five TD-DFT functionals in predicting the adiabatic excitation energy of ZnPr using 6-31G(d,p) basis set.

TABLE 6 | Bond lengths (in Å) of the ZnPr/graphene system obtained from geometry optimization at the ωB97XD/CPCM (chloroform) level using different basis sets.

Basis set	C–C$_{graphene}$	C–C$_{ring}$	Zn–C$_{graphene}$
3-21G	1.500	1.456	3.200
6-31G(d.p)	1.413	1.458	3.340
6-311G(d.p)	1.422	1.457	3.350
6-311G+(d.p)	1.434	1.458	3.360
6-31G(d)/ LANL2DZ	1.400	1.460	3.350
6-31G(d.p)/ LANL2DZ	1.411	1.460	3.350
6-311G(d)/ LANL2TZ	1.412	1.459	3.340
6-311G(d.p)/ LANL2TZ	1.423	1.459	3.340
cc-PVDZ	1.361	1.456	3.350
cc-PVTZ	1.362	1.455	3.340
Def2-TZVP	1.425	1.450	3.390
6-31G(d)/ Def2-TZVP*	1.422	1.447	3.410
DRX [64, 65]	1.421	1.449	3.420

Note: Experimental data from single-crystal x-ray diffraction are included for comparison [64, 65].

with the absorption of light polarized along different axes in a material; Q_x represents transitions polarized along the *x*-axis while Q_y represents transitions polarized along the *y*-axis. These are located in the visible range 500–600 nm corresponding to the first two excited states. M06 and M06-2X hybrid density functionals provide an overestimation description of the vertical excitation energy values E_v, with MAD values of 0.32

and 0.27 eV, respectively. A similar situation is found for the B3LYP and CAM-B3LYP density functionals with MAD values of 0.21 and 0.19 eV, respectively. The reasons for such deviations are unclear and probably originate from the several approximations in these functionals, posing challenges in the modeling of these types of systems [61–63].

Once the suited density functional is chosen, we focus now on the basis set. Thus, different basis sets were analyzed to find out the most suitable one providing geometric data close to the experimental available data [64, 65]. An interesting feature in the pigment structure adsorbed over graphene is the length of the Zn–C bond, which in our system varies between 1.320 and 1.335 Å (see Table 6). The best matching between our computational analysis and experimental data is achieved when employing the 6-31G(d)/Def2-TZVP basis set combination as found in the literature for other organic pigments adsorbed on graphene [66–68]. This is because larger basis sets provide more reliable geometries [69] and are essential for achieving accurate results in post-Hartree–Fock calculations [70]. Once the structure is obtained, we analyzed the striking absorption spectra of ZnPc and ZnPr adsorbed on graphene at the TD-DFT level using the ωB97XD/6-31G(d) functional and the sufficiently large Def2-TZVP basis set.

Owing to their intricate conjugated structures, the simulated UV spectra of ZnPc/G and ZnPr/G reported in Figure 5 exhibit two discernible bands characterized by intense absorption within the visible spectrum. These bands include a prominent Soret band, centered roughly between 400 and 500 nm, and a Q band spanning the 550–650 nm range, rendering the molecules deeply pigmented. The robust Soret band in ZnPr (approximately at ~350 nm) corresponds to the electronic transition from the highest occupied molecular orbital (HOMO) to the lowest unoccupied molecular orbital (LUMO), indicative of π–π^* interactions. Conversely, the moderate intensity of the Q band (around ~500 nm) suggests potential involvement in charge-transfer phenomena, including charge-transfer (CT),

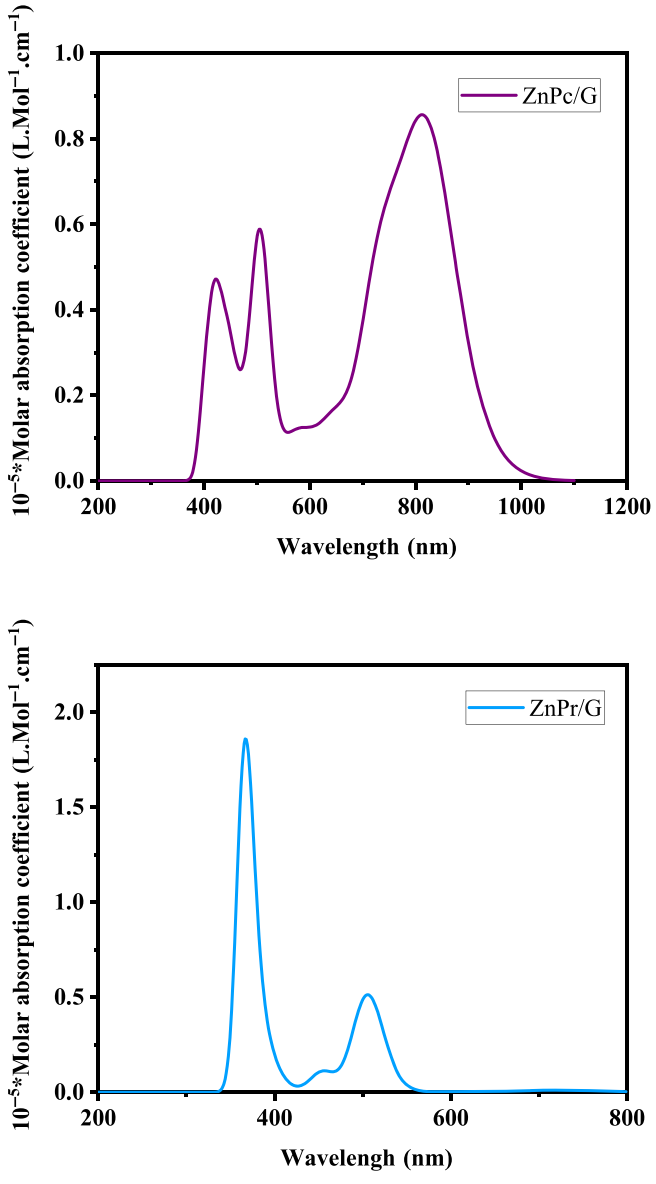

FIGURE 5 | Simulated UV–vis absorption spectra of ZnPc/G (purple) and ZnPr/G (sky blue) as predicted from TDDFT at the ω-B97XD/6-31G(d)/Def2-TZVP/CPCM (chloroform) level.

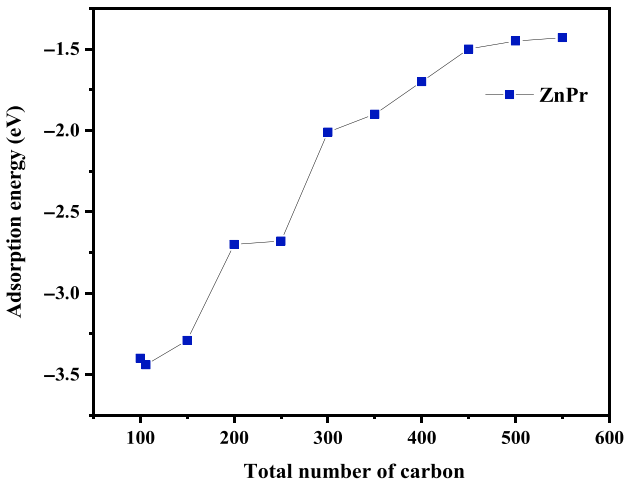

FIGURE 6 | Variation of adsorption energy of ZnPr with the size of graphene flake.

TABLE 7 | Adsorption energies E_{ads}, basis set superposition error energy, E^{BSSE}, and corrected adsorption energies E_{ads}^{BSSE} calculated in (eV) for MPr (M = Zn, Cd, Hg, Pd, Pt, Rh, Ir, Ru, Os) attached to the graphene surface at the ωB97XD/6-31G(d)/Def2-TZVP/CPCM (chloroform) level.

Metal	E_{ads}	E^{BSSE}	E_{ads}^{BSSE}
Zn	−0.149	0.057	−0.092
Cd	−0.166	0.072	−0.094
Hg	−0.164	0.071	−0.093
Pd	−0.146	0.060	−0.086
Pt	−0.148	0.061	−0.087
Rh	−0.108	0.046	−0.062
Ir	−0.110	0.047	−0.063
Ru	−0.071	0.019	−0.052
Os	−0.072	0.018	−0.054

metal-to-ligand charge-transfer (MLCT), ligand-to-ligand charge-transfer (LLCT), and metal-centered (MC) transitions, as elucidated by previous studies [71]. In the case of ZnPc/G, the spectrum predominantly showcases π–π^* transitions without significant contribution from charge transfer mechanisms. Furthermore, the analysis of UV–visible spectra revealed that the absorbance values do not affect the adsorption of molecules on graphene, compared to isolated systems. This finding represents a promising result that fully justifies the use of graphene as a support.

3.3 | The Effect of the Central Atom

Finally, we analyze the effect of the central atom composing the porphyrins on the adsorption energy. Numerous experimental studies have been conducted on the synthesis of materials based on porphyrins adsorbed on graphene. For example, Xu et al. [72] successfully synthesized a porphyrin/graphene material demonstrating interesting optical properties such as enhanced light absorption, nonlinear optical response, broad absorption spectrum, and covalent functionalization. The authors suggested that this material could represent a promising advancement in the field of light-harvesting devices. Therefore, we here study the adsorption energy of porphyrin derivatives on a graphene surface using a finite flake as a model. As depicted in Figure 6, we observe that the adsorption energies increase monotonically with the size of the graphene, due to the increased dispersion interaction [73].

The dimensions of the studied system are characterized by a single layer of *sp* [2] hybridized carbon atoms arranged in a hexagonal lattice with a lattice constant of approximately 0.246 nm. The effect of the central metal atom on the adsorption energy (E_{ads}) is summarized in Table 7. The type of central metal exerts a subtle influence on E_{ads}, although this is very weak in all cases. The observed stability order, with the sequence being CdPr > HgPr > ZnPr > PtPr > PdPr > IrPr > RhPr > OsPr > RuPr, seems to indicate that the larger the occupancy of the valence *d* shell, the larger the interaction as these are quite polarizable electrons. The use of Cd and Hg atoms within the porphyrin structure leads to the most favorable adsorption energy. Building upon prior findings regarding isolated systems, it is evident that porphyrins containing cadmium and mercury demonstrate superior oscillator strength values compared to other studied metals, except for zinc. This suggests that Cd and Hg-based porphyrins offer enhanced light-harvesting efficiency (LHE) and overall performance [48]. This finding suggests a promising direction for optimizing the adsorption process in related applications and could serve as a valuable guide for optimizing the design of these complexes to simultaneously enhance solar cell efficiency and the capture of heavy metals.

This finding suggests a promising direction for optimizing the adsorption process in related applications and could serve as a valuable guide for optimizing the design of these complexes to simultaneously enhance solar cell efficiency and the capture of heavy metals.

4 | Conclusion

In this study, the adsorption of phthalocyanines and porphyrins on a graphene surface has been investigated. A first analysis based on the evaluation of experimental geometric parameters, and optical and electronic properties showed that a simplification of the atomic models is possible when studying these pigments form a computational viewpoint, without losing relevant information. The present results demonstrated that the ωB97XD functional combined with 31G(d)/Def2-TZVP basis set provides an excellent choice to lead accurate results in this type of system, supported by comparing with experiments.

The use of graphene as an adsorption surface does not significantly influence the absorption properties and light harvesting efficiency in the UV–visible region of the electromagnetic spectrum. The spectra reveal intense bands, suggesting potential involvement in charge transfer phenomena, and offer a promising avenue for designing hybrid materials with specific functionalities for various applications.

The adsorption energies of metalloporphyrins on graphene flakes were also considered. This increases monotonically with the size of the graphene model and converges for models containing over 500 atoms. The cadmium and mercury-based complexes exhibit promising efficiency values as solar power harvesters, aided by their adsorption on graphene. They also hold potential as candidates for applications related to the capture and extraction of heavy metals like cadmium and mercury.

Acknowledgments

We thank the financial support from MCIN/AEI/10.13039/501100011033 through projects PID2020-115293RJ-I00, PID2021-126076NB-I00, TED2021-129506B-C22, and the *Maria de Maeztu* CEX2021-001202-M project, and, in part, from the *Generalitat de Catalunya* through the 2021-SGR-00079 grant. The reported research is also involved in the European Cooperation in Science and Technology (COST) Actions: CA18234.

Data Availability Statement

The data that support the findings of this study are available from the corresponding author upon reasonable request.

References

1. F. Zhang, K. Yang, G. Liu, et al., "Recent Advances on Graphene: Synthesis, Properties and Applications," *Composites Part A: Applied Science and Manufacturing* 160 (2022): 107051.

2. G. Yildiz, M. Bolton-Warberg, and F. Awaja, "Graphene and Graphene Oxide for Bio-Sensing: General Properties and the Effects of Graphene Ripples," *Acta Biomaterialia* 131 (2021): 62–79.

3. H. Qiao, H. Liu, Z. Huang, et al., "Tunable Electronic and Optical Properties of 2D Monoelemental Materials Beyond Graphene for Promising Applications," *Energy and Environmental Materials* 4 (2021): 522–543.

4. A. Kumar, K. Sharma, and A. R. Dixit, "A Review on the Mechanical Properties of Polymer Composites Reinforced by Carbon Nanotubes and Graphene," *Carbon Letters* 31 (2021): 149–165.

5. J. Touzeau, F. Barbault, F. Maurel, and M. Seydou, "Insights on Porphyrin-Functionalized Graphene: Theoretical Study of Substituent and Metal-Center Effects on Adsorption," *Chemical Physics Letters* 713 (2018): 172–179.

6. Y.-H. Zhang, K.-G. Zhou, K.-F. Xie, J. Zeng, H.-L. Zhang, and Y. Peng, "Tuning the Electronic Structure and Transport Properties of Graphene

by Noncovalent Functionalization: Effects of Organic Donor, Acceptor and Metal Atoms," *Nanotechnology* 21 (2010): 065201.

7. C.-H. Chang, X. Fan, L.-J. Li, and J.-L. Kuo, "Band Gap Tuning of Graphene by Adsorption of Aromatic Molecules," *Journal of Physical Chemistry C* 116 (2012): 13788–13794.

8. J. M. MacLeod, J. A. Lipton-Duffin, D. Cui, S. De Feyter, and F. Rosei, "Substrate Effects in the Supramolecular Assembly of 1,3,5-Benzene Tricarboxylic Acid on Graphite and Graphene," *Langmuir* 31 (2015): 7016–7024.

9. H. Medina, Y. Lin, D. Obergfell, and P. Chiu, "Tuning of Charge Densities in Graphene by Molecule Doping," *Advanced Functional Materials* 21 (2011): 2687–2692.

10. B. Sekaran and R. Misra, "β-Pyrrole Functionalized Porphyrins: Synthesis, Electronic Properties, and Applications in Sensing and DSSC," *Coordination Chemistry Reviews* 453 (2022): 214312.

11. M. Yahya, Y. Nural, and Z. Seferoğlu, "Recent Advances in the Nonlinear Optical (NLO) Properties of Phthalocyanines: A Review," *Dyes and Pigments* 198 (2022): 109960.

12. S. Huang, K. Chen, and T.-T. Li, "Porphyrin and Phthalocyanine Based Covalent Organic Frameworks for Electrocatalysis," *Coordination Chemistry Reviews* 464 (2022): 214563.

13. Y. Zhang, T. Higashino, and H. Imahori, "Molecular Designs, Synthetic Strategies, and Properties for Porphyrins as Sensitizers in Dye-Sensitized Solar Cells," *Journal of Materials Chemistry A* 11 (2023): 12659–12680.

14. J. E. Durantini, R. Rubio, C. Solis, et al., "Electrosynthesis of a Hyperbranched Dendrimeric Porphyrin Polymer: Optical and Electronic Characterization as a Material for Bifunctional Electrochromic Supercapacitors," *Sustainable Energy & Fuels* 4 (2020): 6125–6140.

15. A. Sarkar, A. B. Rahaman, K. Chakraborty, T. Pal, S. Ghosh, and D. Banerjee, "Organic Heterojunctions of Phthalocyanine-Reduced Graphene Oxide Above Percolation Threshold for Photovoltaic Application," *Materials Chemistry and Physics* 253 (2020): 123418.

16. M. C. Vebber, T. M. Grant, J. L. Brusso, and B. H. Lessard, "Bis(Trialkylsilyl Oxide) Silicon Phthalocyanines: Understanding the Role of Solubility in Device Performance as Ternary Additives in Organic Photovoltaics," *Langmuir* 36 (2020): 2612–2621.

17. F. Farjadian, S. Abbaspour, M. A. A. Sadatlu, et al., "Recent Developments in Graphene and Graphene Oxide: Properties, Synthesis, and Modifications: A Review," *ChemistrySelect* 5 (2020): 10200–10219.

18. R. Gara, M. O. Zouaghi, and Y. Arfaoui, "Porphyrin and Phthalocyanine Heavy Metal Removal: Overview of Theoretical Investigation for Heterojunction Organic Solar Cell Applications," *Journal of Molecular Modeling* 29 (2023): 259.

19. V. Thanabal and V. Krishnan, "Porphyrins With Multiple Crown Ether Voids: Novel Systems for Cation Complexation Studies," *Journal of the American Chemical Society* 104 (1982): 3643–3650.

20. O. Yavuz, Y. Alcay, K. Kaya, et al., "Superior Sensor for Be^{2+} Ion Recognition via the Unprecedented Octahedral Crystal Structure of a One-Dimensional Coordination Polymer of Crown Fused Zinc Phthalocyanine," *Inorganic Chemistry* 58 (2018): 909–923.

21. S. Z. Topal, D. Atilla, K. Ertekin, et al., "Investigation of Optical and Electrochemical Properties as Well as Metal Ion Sensitivities of Different Number of Crown Ether Appended Phthalocyanines," *Phthalocyanines* 17 (2013): 682–690.

22. M. J. Frisch, G. W. Trucks, H. B. Schlegel, et al., *Gaussian 16, Revision C.01* (Wallingford, CT: Gaussian Inc, 2016).

23. R. Dennington, T. A. Keith, and J. M. Millam, *GaussView Version 6* (Shawnee Mission, KS: Semichem Inc, 2016), http://Gaussian.Com/Uvvisplot.

24. A. D. Becke, "Density-Functional Thermochemistry. III. The Role of Exact Exchange," *Journal of Chemical Physics* 98 (1993): 5648–5652.

25. P. J. Stephens, F. J. Devlin, C. F. Chabalowski, and M. J. Frisch, "Ab Initio Calculation of Vibrational Absorption and Circular Dichroism Spectra Using Density Functional Force Fields," *Journal of Physical Chemistry* 98 (1994): 11623–11627.

26. T. Yanai, D. P. Tew, and N. C. Handy, "A New Hybrid Exchange–Correlation Functional Using the Coulomb-Attenuating Method (CAM-B3LYP)," *Chemical Physics Letters* 393 (2004): 51–57.

27. Y. Zhao and D. G. Truhlar, "The M06 Suite of Density Functionals for Main Group Thermochemistry, Thermochemical Kinetics, Noncovalent Interactions, Excited States, and Transition Elements: Two New Functionals and Systematic Testing of Four M06-Class Functionals and 12 Other Functionals," *Theoretical Chemistry Accounts* 120 (2008): 215–241.

28. M. Doust Mohammadi and H. Y. Abdullah, "The Adsorption of Chlorofluoromethane on Pristine, and Al- and Ga-Doped Boron Nitride Nanosheets: A DFT, NBO, and QTAIM Study," *Journal of Molecular Modeling* 26 (2020): 287.

29. L. G. Gutsev, S. M. Aldoshin, and G. L. Gutsev, "Influence of Back Donation Effects on the Structure of ZnO nanoclusters," *Journal of Computational Chemistry* 41 (2020): 2583–2590.

30. G. Gocheva, N. Petkov, A. Garcia Luri, et al., "Tautomerism in Folic Acid: Combined Molecular Modelling and NMR Study," *Journal of Molecular Liquids* 292 (2019): 111392.

31. J. V. Teixeira Gomes, A. C. P. Da Silva, M. L. Bello, C. R. Rodrigues, and B. A. M. C. Santos, "Molecular Modeling as a Design Tool for Sunscreen Candidates: A Case Study of Bemotrizinol," *Journal of Molecular Modeling* 25 (2019): 362.

32. G. Días da Silva, R. L. O. R. Cunha, and M. D. Coutinho-Neto, "Equilibrium Between Tri- and Tetra-Coordinate Chalcogenuranes Is Critical for Cysteine Protease Inhibition," *Journal of Computational Chemistry* 42 (2021): 1225–1235.

33. C. V. Santos, G. M. B. Da Silva, R. P. Dias, R. T. Moura, and J. C. S. Da Silva, "ExploringTransEffect Concept in Pt(II) Complexes Through the Quantum Theory of Atoms in Molecules and Chemical Bond Overlap Model Perspectives," *Advanced Theory and Simulations* 7 (2024): 2470011.

34. R. Su and Z. Huang, "A Series of Singlet-Triplet Inverted TADF Fluorescent Probes With High Stability, Low Molecular Weight, and Synthesis Accessibility," *Advanced Theory and Simulations* 6 (2023): 2200863.

35. I. H. S. Ribeiro, D. T. Reis, and D. H. Pereira, "A DFT-Based Analysis of Adsorption of Cd^{2+}, Cr^{3+}, Cu^{2+}, Hg^{2+}, Pb^{2+}, and Zn^{2+}, on Vanillin Monomer: A Study of the Removal of Metal Ions From Effluents," *Journal of Molecular Modeling* 25 (2019): 267.

36. I. de Matos Mourão, A. L. P. Neto, A. A. Silva, J. de Tanaka, and J. G. Varela, "Density Functional Theory Study of Interactions Between Carbon Monoxide and Iron Tetraaza Macrocyclic Complexes, FeTX-TAA (X = −Cl, −OH, $-OCH_3$, $-NH_2$, and $-NO_2$)," *Journal of Molecular Modeling* 23 (2017): 64.

37. E. Titov and A. Beqiraj, "Exciton States of Azobenzene Aggregates: A First-Principles Study," *Advanced Theory and Simulations* 6 (2023): 2200907.

38. S. Miertuš, E. Scrocco, and J. Tomasi, "Electrostatic Interaction of a Solute With a Continuum. A Direct Utilizaion of AB Initio Molecular Potentials for the Prevision of Solvent Effects," *Chemical Physics* 55 (1981): 117–129.

39. M. Cossi, N. Rega, G. Scalmani, and V. Barone, "Energies, Structures, and Electronic Properties of Molecules in Solution With the C-PCM Solvation Model," *Journal of Computational Chemistry* 24 (2003): 669–681.

40. A. Haloui and Y. Arfaoui, "A DFT Study of the Conformational Behavior of Para-Substituted Acetophenones in Vacuum and in Various Solvents," *THEOCHEM Journal of Molecular Structure* 950 (2010): 13–19.

41. P. S. Liyanage, R. M. De Silva, and K. M. N. De Silva, "Nonlinear Optical (NLO) Properties of Novel Organometallic Complexes: High Accuracy Density Functional Theory (DFT) Calculations," *THEOCHEM Journal of Molecular Structure* 639 (2003): 195–201.

42. R. Gara, M. O. Zouaghi, L. M. H. ALshandoudi, and Y. Arfaoui, "DFT Investigation of Solvent, Substituent, and Catalysis Effects on the Intramolecular Diels–Alder Reaction," *Journal of Molecular Modeling* 27 (2021): 125.

43. R. Omrani, M. O. Zouaghi, and Y. Arfaoui, "Mechanistic Density Functional Theory Study of the Claisen Rearrangement Diels–Alder Cycloaddition Domino Sequence for the Synthesis of the Caged Garcinia Xanthone," *Journal of Molecular Structure* 1202 (2020): 127305.

44. M. E. Casida, "Time-Dependent Density Functional Response Theory for Molecules," in *Recent Advances in Computational Chemistry* (Singapore: World Scientific, 1995), 155–192.

45. R. Bauernschmitt and R. Ahlrichs, "Treatment of Electronic Excitations Within the Adiabatic Approximation of Time Dependent Density Functional Theory," *Chemical Physics Letters* 256 (1996): 256–464.

46. D. J. Tozer and N. C. Handy, "Improving Virtual Kohn–Sham Orbitals and Eigenvalues: Application to Excitation Energies and Static Polarizabilities," *Journal of Chemical Physics* 109 (1998): 10180–10189.

47. S. Gautier, S. N. Steinmann, C. Michel, P. Fleurat-Lessard, and P. Sautet, "Molecular Adsorption at Pt(111). How Accurate Are DFT Functionals?," *Physical Chemistry Chemical Physics* 17 (2015): 28921–28930.

48. S. F. Boys and F. Bernardi, "The Calculation of Small Molecular Interactions by the Differences of Separate Total Energies. Some Procedures With Reduced Errors," *Molecular Physics* 19 (1970): 553–566.

49. H. M. Badran, K. M. Eid, and H. Y. Ammar, "DFT and TD-DFT Studies of Halogens Adsorption on Cobalt-Doped Porphyrin: Effect of the External Electric Field," *Results in Physics* 23 (2021): 103964.

50. Y. Zhang, Y.-W. Tan, H. L. Stormer, and P. Kim, "Experimental Observation of the Quantum Hall Effect and Berry's Phase in Graphene," *Nature* 438 (2005): 201–204.

51. L.-Y. Cui, J. Yang, Q. Fu, B.-Z. Zhao, L. Tian, and H.-L. Yu, "Synthesis, Crystal Structure and Characterization of a New Zinc Phthalocyanine Complex," *Journal of Molecular Structure* 827 (2007): 149–154.

52. Y. Terazono, B. O. Patrick, and D. H. Dolphin, "Synthesis, Crystal Structures, and Redox Potentials of 2,3,12,13-Tetrasubstituted 5,10,15,20-Tetraphenylporphyrin Zinc(II) Complexes," *Inorganic Chemistry* 41 (2002): 6703–6710.

53. S. Sahu and G. C. Rout, "Band Gap Opening in Graphene: A Short Theoretical Study," *International Nano Letters* 7 (2017): 81–89.

54. G. Cárdenas-Jirón, M. Borges-Martínez, E. Sikorski, and T. Baruah, "Excited States of Light-Harvesting Systems Based on Fullerene/Graphene Oxide and Porphyrin/Smaragdyrin," *Journal of Physical Chemistry C* 121 (2017): 4859–4872.

55. P. N. Samanta and K. K. Das, "Structural and Electronic Properties of Covalently Functionalized 2-Aminoethoxy-Metallophthalocyanine-Graphene Hybrid Materials: A Computational Study," *RSC Advances* 5 (2015): 85730–85740.

56. J. P. Perdew, K. Burke, and M. Ernzerhof, "Generalized Gradient Approximation Made Simple," *Physical Review Letters* 77 (1996): 3865–3868.

57. S. Grimme, J. Antony, S. Ehrlich, and H. Krieg, "A Consistent and Accurateab Initioparametrization of Density Functional Dispersion Correction (DFT-D) for the 94 Elements H–Pu," *Journal of Chemical Physics* 132 (2010): 154104.

58. J. D. Correa and W. Orellana, "Optical Response of Carbon Nanotubes Functionalized With (Free-Base, Zn) Porphyrins, and Phthalocyanines: A DFT Study," *Physical Review B* 86 (2012): 125417.

59. R. Seoudi, G. S. El-Bahy, and Z. A. El Sayed, "Ultraviolet and Visible Spectroscopic Studies of Phthalocyanine and Its Complexes Thin Films," *Optical Materials* 29 (2006): 304–312.

60. A. V. Zamyatin, A. V. Soldatova, and M. A. J. Rodgers, "The Photophysics of Ni(II) Meso-Tetraphenylbenzoporphyrin: A Combined Theoretical and Experimental Investigation," *Inorganica Chimica Acta* 360 (2007): 857–868.

61. B. Champagne, E. A. Perpète, S. J. A. Van Gisbergen, et al., "Assessment of Conventional Density Functional Schemes for Computing the Polarizabilities and Hyperpolarizabilities of Conjugated Oligomers: Anab Initioinvestigation of Polyacetylene Chains," *Journal of Chemical Physics* 109 (1998): 10489–10498.

62. H. Appel, E. K. U. Gross, and K. Burke, "Excitations in Time-Dependent Density-Functional Theory," *Physical Review Letters* 90 (2003): 043005.

63. A. Dreuw, J. L. Weisman, and M. Head-Gordon, "Long-Range Charge-Transfer Excited States in Time-Dependent Density Functional Theory Require Non-Local Exchange," *Journal of Chemical Physics* 119 (2003): 2943–2946.

64. D. Li, S. Ge, T. Yuan, et al., "Green Synthesis and Characterization of Crystalline Zinc Phthalocyanine and Cobalt Phthalocyanine Prisms by a Simple Solvothermal Route," *CrystEngComm* 20 (2018): 2749–2758.

65. M. Zhu, C. Cao, J. Chen, et al., "Electronic Tuning of Cobalt Porphyrins Immobilized on Nitrogen–Doped Graphene for CO_2 Reduction," *ACS Applied Energy Materials* 2 (2019): 2435–2440.

66. E. Gacka, G. Burdzinski, B. Marciniak, A. Kubas, and A. Lewandowska-Andralojc, "Interaction of Light With a Non-Covalent Zinc Porphyrin–Graphene Oxide Nanohybrid," *Physical Chemistry Chemical Physics* 22 (2020): 13456–13466.

67. E. Gacka, A. Wojcik, M. Mazurkiewicz-Pawlicka, et al., "Noncovalent Porphyrin–Graphene Oxide Nanohybrids: The pH-Dependent Behavior," *Journal of Physical Chemistry C* 123 (2019): 3368–3380.

68. D. Cortés-Arriagada and D. E. Ortega, "Effects on the Aromatic Character of DNA/RNA Nucleobases Due to Its Adsorption Onto Graphene," *International Journal of Quantum Chemistry* 118 (2018): e25699.

69. T. Helgaker, W. Klopper, H. Koch, and J. Noga, "The Coupled–Cluster Approach to Molecular Structure and Spectroscopy," *Chemical Physics Letters* 328 (2000): 805–813.

70. T. H. Dunning, "Gaussian Basis Sets for Use in Correlated Molecular Calculations. I. The Atoms Boron Through Neon and Hydrogen," *Journal of Chemical Physics* 90 (1989): 1007–1023.

71. J. Jing, J. Yang, Z. Zhang, and Y. Zhu, "Supramolecular Zinc Porphyrin Photocatalyst With Strong Reduction Ability and Robust Built-in Electric Field for Highly Efficient Hydrogen Production," *Advanced Energy Materials* 11, no. 29 (2021): 2101392.

72. Y. Xu, Z. Liu, X. Zhang, et al., "A Graphene Hybrid Material Covalently Functionalized With Porphyrin: Synthesis and Optical Limiting Property," *Advanced Materials* 21, no. 12 (2009): 1275–1279.

73. Y. Kanematsu, K. Gohara, H. Yamada, and Y. Takano, "Applicability of Density Functional Tight Binding Method With Dispersion Correction to Investigate the Adsorption of Porphyrin/Porphycene Metal Complexes on Graphene," *Chemistry Letters* 46, no. 1 (2017): 51–52.